EFDA–JET–CP(10)03/13

L. Figini, S. Garavaglia, E. De La Luna, D. Farina, P. Platania, A. Simonetto,
C. Sozzi, and JET EFDA contributors

Measure of EC Emission at Multiple Angles in High Te Plasmas of JET

Measure of EC Emission at Multiple Angles in High Te Plasmas of JET

L. Figini[1], S. Garavaglia[1], E. De La Luna[2,3], D. Farina[1], P. Platania[1], A. Simonetto[1], C. Sozzi[1], and JET EFDA contributors*

JET-EFDA, Culham Science Centre, OX14 3DB, Abingdon, UK

[1]Istituto di Fisica del Plasma CNR, Euratom-ENEA-CNR Association, 20125 Milano, Italy
[2]Asociación EURATOM-CIEMAT, Avenida Complutense 22, E-28040 Madrid, Spain
[3]EFDA-CSU, Culham Science Centre, OX14 3DB, Abingdon, OXON, UK
** See annex of F. Romanelli et al, "Overview of JET Results",*
(Proc. 22 [nd] IAEA Fusion Energy Conference, Geneva, Switzerland (2008)).

Preprint of Paper to be submitted for publication in Proceedings of the
18th High Temperature Plasma Diagnostics, Wildwood, New Jersey, USA.
(16th May 2010 - 20th May 2010)

ABSTRACT.
The Oblique ECE diagnostic installed at JET allows simultaneous analysis of the ECE spectra along three lines of sight (with toroidal angles 0^o, ~10^o, ~20^o) and 2 linear polarizations for each oblique line of sight. Capable of measuring EC emission over the band 75-800GHz with 5ms time resolution and 7.5GHz spectral resolution, the diagnostic is designed to investigate the features of ECE spectra related to electron distribution in the thermal velocity range. Instrumental accuracy was assessed using sources at different temperatures (77−900K) and with plasma emission. ECE from high temperature plasmas and in presence of fast ions has been compared to simulations performed with the modeling code SPECE, putting an upper limit to possible discrepancies from thermal emission.

1. INTRODUCTION

The multiple angles Electron Cyclotron Emission (ECE) diagnostic [1] of the Joint European Torus (JET) was designed with the specific purpose of investigating and identifying possible not-Maxwellian features in the electron distribution function, particularly in the thermal and sub-thermal energy range. The motivation was given by the discrepancies observed between Thomson scattering and ECE measurements of the electron temperature T_e in plasmas with strong auxiliary heating [2]. The angles between the lines of sight and the magnetic field have been optimized to obtain a good coverage of the velocity space in the thermal energy range. However, the wide spectral coverage allows the detection of EC emission also at frequencies at which the plasma is optically thin, and emission by fast electrons, like those generated by interaction with Lower Hybrid waves, is thus easily measurable too.

As a support to the diagnostic, the raytracing code SPECE3 was developed, and it has been used extensively both during the phase of characterization of the instrument and for measured data interpretation.

In section 2 a brief description of the instrument is given, section 3 describes the work done to determine the instrumental response, and to assess the noise level, while a set of high T_e ECE spectra measured at JET are shown and compared with the spectra predicted by the code SPECE in section 4. Conclusions are eventually drawn in section 5.

2. INSTRUMENT DESCRIPTION

The diagnostic measures the EC emission along three lines of sight and for two orthogonal linear polarizations (mostly X-,mostly O-mode). A rectangular waveguide collects radially propagating EC radiation from a radial coordinate R_{ant} ~ 4.1m, while two circular smooth waveguide antennas collect the radiation at about 9.5^o and 20.5^o respect to the radial direction, at R_{ant}~ 4.3m. Oblique detection is achieved with a combination of fixed mirrors, feeding the nearly radially oriented waveguides. Neglecting refraction effects, the approximate value of the effective angles β_0 between the radial direction and the lines of sight at the plasma centre radius R_0 ~ 3m can be obtained from the relation Rant $\sin(\beta_{ant}) = R_0 \sin(\beta_0)$, giving approximately 14^o and 30.5^o for the two oblique antennas.

All the antennas are located on the low field side of the machine, approximately on the vessel equatorial plane, and are connected to a multi-channel spectrometer by means of ~60m long waveguides. The signal coming from each oblique antenna is split into two orthogonal polarizations, corresponding to quasi-O and quasi-X mode (horizontal and vertical polarization at the antenna, respectively), feeding each one a different channel of the spectrometer. The X-mode polarized perpendicular antenna feeds a fifth channel. All the channels have a similar optical layout, and are essentially one Martin-Puplett interferometer each (figure 1).

The movable arm of the interferometer consists of four helicoidal sectors, with a slope $\alpha = 4.85^{o}$, mounted on a rotating wheel of radius R = 150mm. The recombined output beam is sent through a waveguide to a broadband He cooled InSb detector. The time trace of the detected signal gives an interference figure of the incoming radiation at every scan of a wheel sector, and a Fourier analysis of the interference figure gives finally the frequency spectrum of the measured signal.

Every wheel rotation corresponds to four complete scans performed by the interferometer, and the optical path difference between the two extremes of the scan is approximately $\Delta x = 2R\ \pi/2\ \sin(\alpha) \approx 40$mm, corresponding to an equivalent spectral resolution of $\delta f = c/\Delta x \approx 7.5$GHz. The five used channels produce independent simultaneous spectra with time resolution up to $\delta t \sim 5$ms (usually 7.5ms for 2000 rpm of the rotating mirror) and with N = 256 samples per wheel sector, the Nyquist frequency is $f_{Nyq} = N/2\ c/\Delta x \approx 960$GHz, guaranteeing the whole spectral coverage from the 1st to the 4th harmonic (75-350GHz for a magnetic field B ≈ 3T).

3. CALIBRATION

A. Calibration Technique

As described in the previous section, the frequency power spectrum $U_n(f)$ of the signal detected by the n-th channel is obtained as Fourier transformation of the respective interference figure $V_n(x)$ acquired during a scan îx in the position of the movable mirror. Once the instrument response function $g_n(f)$ (the calibration function) has been determined for each channel, the calibrated EC spectrum $I_n(f)$ can be extracted from the measured signal as $I_n(f) = U_n(f) / g_n(f)$. For each frequency value in the spectral range of JET EC emission (75-350GHz) the calibration functions $g_n(f)$ are derived by comparing the measured spectrum with a reference spectrum $I_{ref,n}(f)$ in different conditions. The response function is then computed as

$$g_n(f) = \sum_i \left[w_{n,i}(f)\ \frac{U_{n,i}(f)}{I_{ref,n,i}(f)} \right] \bullet \left[\sum_i w_{n,i}(f) \right]^{-1} \qquad (1)$$

where summation is performed over a set of opportunely chosen times slices, and the weight coefficient $w_{n,i}$ is chosen proportional to the normalized temperature spectrum, in such a way to reduce the contribution of a given time slice at frequencies with limited signal to noise ratio.

The choice of the time slices is in principle arbitrary, but in practical terms three JET pulse-types with magnetic field B and plasma current I_p ramp have been developed on purpose, in order to obtain valuable data over the largest possible frequency range. In those plasmas B and I_p decrease

accordingly maintaining as constant as possible the safety factor and the electron temperature profile shape. A wide scan of the magnetic field, a wide temperature profile and high electron density are ideal conditions to cover a spectral range as large as possible, while minimizing the uncertainties.

The Michelson interferometer perpendicular ECE diagnostic of JET was absolutely calibrated in the past, and it could be used to give the reference spectra for the perpendicular channel. However, the slightly different height of the two antennas on the equatorial plane ($\Delta z \approx 11$cm) is a source of error in the final result, and in any case this procedure can be applied only to the perpendicular line of sight. In order to overcome these limitations, the ECE spectrum seen by the Michelson diagnostic is simulated with SPECE. The input data and the free parameters of the code are adjusted to account for small uncertainties in the equilibrium reconstruction, in the edge density, or in the reflectivity of the vessel walls. Once the simulated spectrum fit properly the calibrated data, the same parameters are used to simulate the emission as seen by the five channels of the multiangle diagnostic, and those spectra are taken as reference for the calibration procedure.

Results have been crosschecked using local blackbody radiation sources (77-900K), even if with a local source the transmission lines attenuation waveguide attenuation are not taken into account.

B. Instrumental Noise

The level of instrumental noise has been assessed computing the average power spectrum of the signal in the first and in the last phase of a few discharges. In these time intervals data acquisition is active, but there is no plasma in the vessel, and the measured signal is thus representative of the background noise level. Figure 2 shows the noise power spectrum measured for the 5 channels in temperature units, compared to typical EC spectra: a signal-to-noise "best case" at high Te (0^o X-mode for the heating phase of Pulse No: 78006) and a "worst case" at low T_e (10^o O-mode for the ohmic phase of Pulse No: 77908).

Over a large fraction of the frequency band (120-320GHz) the noise temperature Tnoise is between 5 and 200eV for all channels. S/N ratio is thus well above unity on the main ECE peaks, and in this frequency range data quality is degraded only at low Te and high harmonics, where EC spectrum decays to noise level. However for f≤100GHz noise can be of the order of the ECE signal for a few channels, especially limiting O-mode measurements on the first harmonic: in these cases time averaging is necessary in order to increase S/N ratio and to obtain reliable ECE measurements.

4. SPECTRA ANALYSIS

A few plasma discharges at high Te have been selected for analysis. The discharges can be divided in three groups, based on the heating scheme applied: i) Deuterium plasma with Neutral Beam Injection (NBI) heating and Ion Cyclotron Resonance Heating (ICRH) on Hydrogen minority (Pulse No's: 78001-78006); ii) High density plasma with high power NBI heating, and no ICRH (Pulse No's: 77904-77915); iii) Deuterium plasma with ICRH heating on 3He minority (Pulse No's: 73760-73769).

The various heating schemes applied generate different fast ion distributions that, by collisions,

heat the electron population and can possibly generate not Maxwellian features in the electron distribution function (e.d.f.). The high electron density and temperature of the selected shots allows strong EC interaction even at high (n=3) harmonics, making the plasma optically thick to X-mode radiation also at high frequency. This is the best situation for the exploitation of a wide-band, multi-angle ECE diagnostic, since EC emission is well localized in space and in velocity space, and the localization is dependent on the harmonic number n, on the wave polarization (O-mode, X-mode), and on the line of sight.

In order to detect possible deviations from a Maxwellian e.d.f., the spectra measured with the multi-angle ECE diagnostic have been compared with the spectra computed with SPECE, assuming a Maxwellian e.d.f. (Figure 3). Te and ne profiles used as input for the simulations were taken from the Michelson interferometer ECE and the Core LIDAR diagnostic respectively, and the free parameters of the code are adjusted with the same criteria discussed in section 3-A.

Figure 4 summarizes the ratios of measured to simulated intensity found for the 5 channels at the frequency of second and third harmonic peaks. There is no obvious trend of measured data away from the simulated spectra. Emission at optically thick harmonics (second harmonic X-mode X2, perpendicular third harmonic X-mode) is within 10% from the expected value for a Maxwellian plasma. An optimization of the Te profiles used for the simulations directly on the perpendicular X2 peak would have given even better consistency among discharges (e.g. removing the systematic shift towards lower ratios in the 78xxx subset). Interpretation of the discrepancies observed at large angle, high harmonic, and in O-mode spectra can be difficult: the limited optical thickness makes the emission less localized, and introduces further uncertainties due to the dependence of the EC spectrum on plasma density, wall reflectivity, and polarization scrambling.

The effective polarization of the oblique channels is at present under investigation: cases with heavily unbalanced emission in O- and X-mode, like Lower Hybrid heated plasmas where the electron suprathermal population generates strong 2nd harmonic downshifted X-mode emission, showed stronger mode mixing than expected, while the total intensity is in line with predictions. This may suggest a level of polarization mixing along the transmission lines of the instrument higher than estimated, and for this reason the polarization evolution along the waveguides is being checked carefully.

CONCLUSIONS

The multi-angle ECE diagnostic has reached a satisfactory level of reliability. Good agreement is found with redundant information for perpendicular channel coming from the Michelson interferometer diagnostic.

A set of high temperature JET plasma discharges have been analyzed to assess the potential of the diagnostic, even if no significant deviation from Maxwellian behavior was evidenced.

Further improvement is expected with the absolute calibration scheduled in June 2010, and better polarization characterization may help to investigate finer effects, currently undetectable.

ACKNOWLEDGEMENTS

This work was supported by EURATOM and carried out within the framework of the European Fusion Development Agreement. The views and opinions expressed herein do not necessarily reflect those of the European Commission.

REFERENCES

[1]. S. Garavaglia, A. Simonetto, C. Sozzi, and JET-EFDA Contributors, Fusion Engineering and Design **82**, 1224 (2007).

[2]. E. de la Luna, V. Krivenski, G. Giruzzi, C. Gowers, R. Prentice, J.M. Travere, M. Zerbini, Review of Scientific Instruments **74**, 1414 (2003).

[3]. D. Farina, L. Figini, P. Platania, and C. Sozzi, Proceedings of the International Conference on Burning Plasma Diagnostics, Varenna, 24-28 September 2007, AIP Conference Proceedings **988**, 128 (2008).

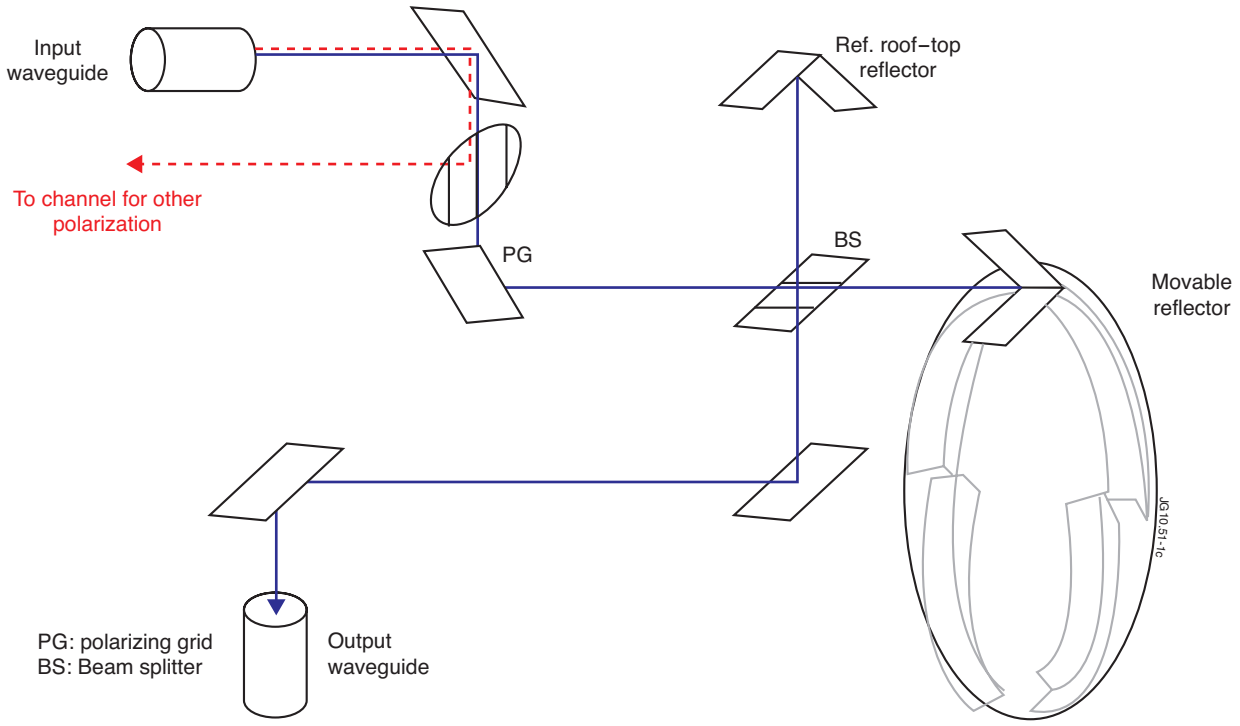

Figure 1: Optical layout for oblique line of sight channels. The configuration for the perpendicular line of sight is conceptually identical.

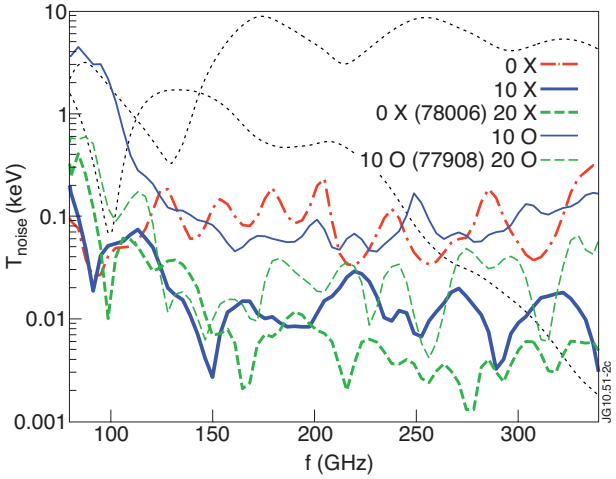

Figure 2: Noise spectrum for the five channels of the instrument, compared with two typical EC spectra at low (77908@13.50s) and high (Pulse No: 78006@9.85) Te.

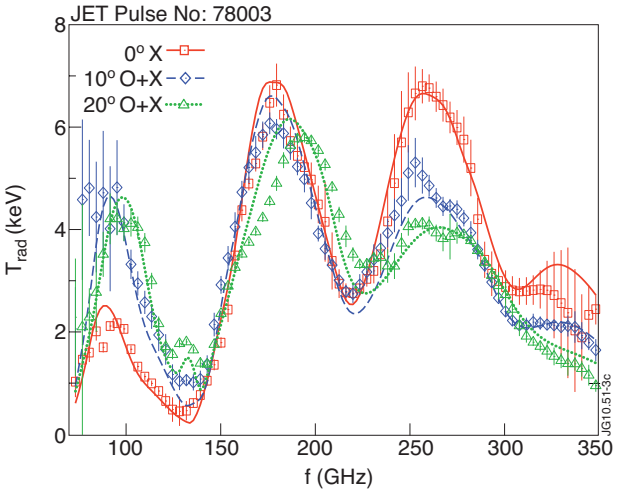

Figure 3: Model/measurements comparison. Oblique spectra are shown as total power (O-mode+X-mode) spectra. Good agreement is found, although large uncertainty at f < 100GHz and some calibration artifacts are visible.

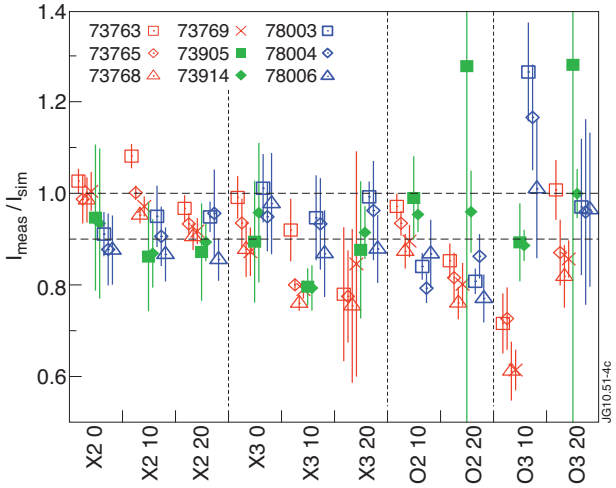

Figure 4: Measured to simulated intensity ratio on 2nd and 3rd harmonic peaks of the 5 measured spectra (perpendicular Xmode, 10 and 20 degrees O-mode and X-mode).